SECOND EUROPEAN CONFERENCE ON EARTHQUAKE ENGINEERING
AND SEISMOLOGY, ISTANBUL AUG. 25-29, 2014

PIPELINE DAMAGE ASSESMENT USING HORIZONTAL DISPLACEMENTS FROM AIR PHOTO AND LiDAR MEASUREMENTS IN AVONSIDE AREA, CHRISTCHURCH, NZ

Selcuk TOPRAK[1], Engin NACAROGLU[2], Thomas D. O'ROURKE[3], A. Cem KOC[4], Masanori HAMADA[5], Misko CUBRINOVSKI[6], Sang-Soo JEON[7]

ABSTRACT

This paper compares displacements measured in Avonside area, Christchurch, NZ, by using two different ways namely air photo and high resolution LiDAR surveys data acquired before and after the 6.2 M_W 22 February 2011 earthquake with respect to their effects on pipeline damage assessments. Avonside area was in the liquefaction zones of the 22 February 2011 earthquake. Where possible, benchmark measurements were also included in the comparisons. In this study, the focus was on AC water pipelines as the length of the pipelines and the number of damages in the study area was much higher compared to other pipe materials, providing sufficient RR data passing the screening criteria to develop linear regressions. The correlations between pipeline damage and lateral ground strains were developed by calculating the horizontal strains from LiDAR and air photo displacements. The results of comparisons are presented and discussed.

INTRODUCTION

Following the 7.1 Mw Sept. 4, 2010 Darfield earthquake, thousands of aftershocks with Mw as high as 6.2 have been recorded in the area of Christchurch, NZ. These earthquakes, termed the Canterbury earthquake sequence are unprecedented in terms of repeated earthquake shocks with substantial levels of ground motion affecting a major city with modern infrastructure. Furthermore, the earthquakes were accompanied by multiple episodes of widespread and severe liquefaction with large PGD levels imposed on underground lifelines during each event. The data collected for the earthquake sequence are likewise unprecedented in size and detail, involving ground motion recordings from scores of seismograph stations, high resolution light detection and ranging (LiDAR) measurements of vertical and lateral movements after each event, and detailed repair records for thousands of km of underground pipelines with coordinates for the location of each repair. In order to determine the effects of ground displacements on pipeline damages air photo and LiDAR measurements were used herein and comparisons were made. High resolution LiDAR data were available through the Canterbury Earthquake Recovery Authority (CERA). Also horizontal and vertical displacements were

[1] Professor, Pamukkale University, Denizli, Turkey, stoprak@pau.edu.tr
[2] Research Assistant, Pamukkale University, Denizli, Turkey, enacaroglu@pau.edu.tr
[3] Professor, Cornell University, Ithaca, NY, USA, tdo1@cornell.edu
[4] Associate Professor, Pamukkale University, Denizli, Turkey, a_c_koc@pau.edu.tr
[5] Professor, Waseda University, Tokyo, Japan, hamada@waseda.jp
[6] Professor, University of Canterbury, Christchurch, New Zealand, misko.cubrinovski@canterbury.ac.nz
[7] Associate Professor, INJE University, Gimhae, South Korea, ssj@inje.ac.kr

available from stereo-pair air photos taken before and after the earthquakes to perform photogrammetric analysis of large ground deformations around Avonside area in Christchurch, NZ. Avonside area was in liquefaction zone.

Geospatial data in the form of GIS maps of the Christchurch water and wastewater distribution systems, locations of pipeline repair, and areas of observed liquefaction effects were integrated into a master GIS file. For the water supply this study focuses on damage to water mains, which are pipelines with diameters typically between 75 and 600 mm, conveying the largest flows in the system. It does not include repairs to smaller diameter submains and customer service laterals. The database was presented in detail and discussed in OôRourke et al. (2012).

Figure 1 shows the water pipelines and repair locations in Avonside area. Also shown in the figure are air photo and LiDAR horizontal displacements. Measurements of lateral movement derived from the LIDAR surveys are provided as displacement in the east-west (EW) and north- south (NS) directions at 56-m intervals. The horizontal spatial accuracy of the LiDAR data is between ± 400 mm and ± 500 mm (CERA, 2012). The data were corrected in this study for tectonic movements, which are also provided through CERA. Horizontal displacements from air photo measurements are provided at 680 locations.

Among the most notable research accomplishments in recent years is the work of Hamada and coworkers (Hamada, et al., 1986; Hamada and OôRourke, 1992) in the use of stereo-pair air photos before and after an earthquake to perform photogrammetric analysis of large ground deformation. This process has influenced the way engineers evaluate soil displacements by providing a global view of deformation that allows patterns of distortion to be quantified and related to geologic and topographic characteristics. The horizontal spatial accuracy of the air photo data in Avonside area is between ± 673 mm and ± 246 mm.

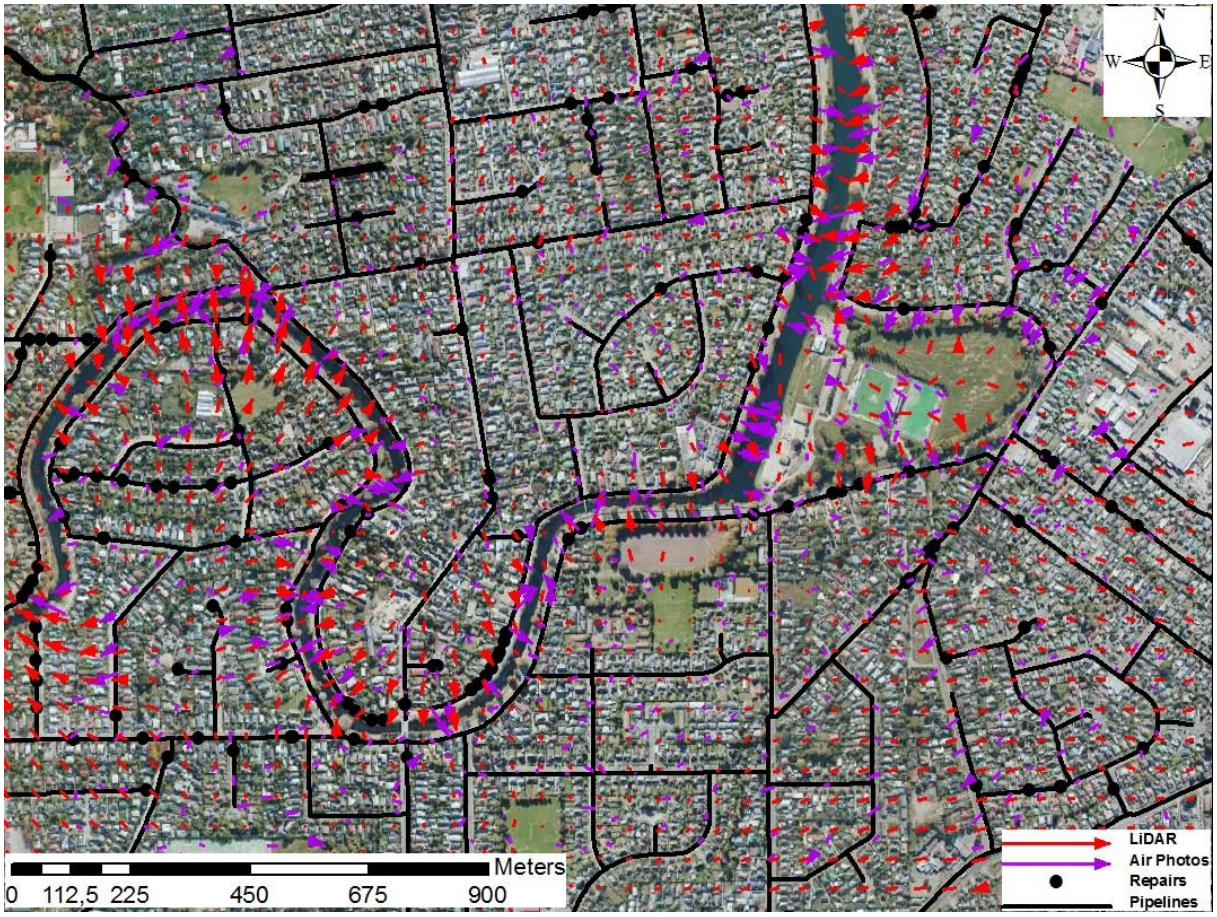

Figure 1. Ground displacement from LiDAR and air photos superimposed on pipelines and pipe repairs in Avonside

There exist some benchmark displacement measurements in Christchurch area after the Canterbury earthquake sequence. Canterbury Geotechnical Database (CGD) provides about 403 benchmarks and their movement relative to earliest survey values after three big earthquakes. These data consist of information from Land Information New Zealand (LINZ), Christchurch City Council, The Earthquake Commission (EQC) and CERA. Figure 2 (LINZ 2014) shows how benchmark looks like and how land movements are measured. There are 25 benchmarks from 403 benchmarks in Avonside area which are used in comparisons with LiDAR and air photos displacements.

This paper compares the results from air photo and LiDAR measurements from Avonside area and discusses their effects on pipeline damage assessment. Where possible, benchmark measurements were also included in the comparisons. For the purpose of horizontal strain calculations, the horizontal displacement data points are considered as corners of square elements. The grid with square elements may be regarded as a finite element mesh with bilinear quadrilateral elements. Knowing the coordinates of each corner and the corresponding displacement, the strains in the EW and NS directions ($\mathring{U}_x$ and $\mathring{U}_y$, respectively) and shear strains ($\mathfrak{I}_{xy}$) can be calculated by computing the spatial derivatives of displacements using linear interpolation. Accordingly, finite element formulations were used to determine horizontal ground strains in the center of the elements, following the method described by Cook (1995). Pipeline repair rates (RRs), repairs/km, corresponding to different strain levels were calculated from air photo and LiDAR lateral movement measurements. Because RR represents damage normalized by available pipe length, the RRs are a good indicator of relative vulnerability (Toprak, et al., 2009; 2011). Then, the repair rates were compared and differences were discussed.

Figure 2. Benchmark measurements (from http://apps.linz.govt.nz/gdb/index.aspx?nextform=image&image_id=108377&mode=&sessionid=115555239158881397733794&code=BDVB)

ANALYSIS

Ground Displacements

As a first stage, LiDAR, air photo and benchmark horizontal ground displacements were compared along the lines shown in Figure 3. The lines were drawn according to existence of both LiDAR and air photo displacement. The beginning and end of the lines are indicated as A and B, respectively. The components of the measured displacements along and perpendicular to any line were calculated for each displacement which was sufficiently close to the line. Then, all parallel and perpendicular displacements for a line compared separately as shown in Figures 4 and 5. It should be noted the displacements in each graph start from zero as the displacement value at the beginning of the line is subtracted from all displacement along the line. So the results are kind of relative displacements with respect to beginning of the line. The results show that there are reasonably good comparison between the displacements measured by LiDAR and air photo for many of the lines. But the differences are quite significant along few lines. Also there is more scatter in air photo displacements. Figure 5 also includes benchmark displacements in the comparisons. When compared with benchmarks, no clear superiority is observed for LiDAR and air photo measurements. However, air photo displacements are more scattered.

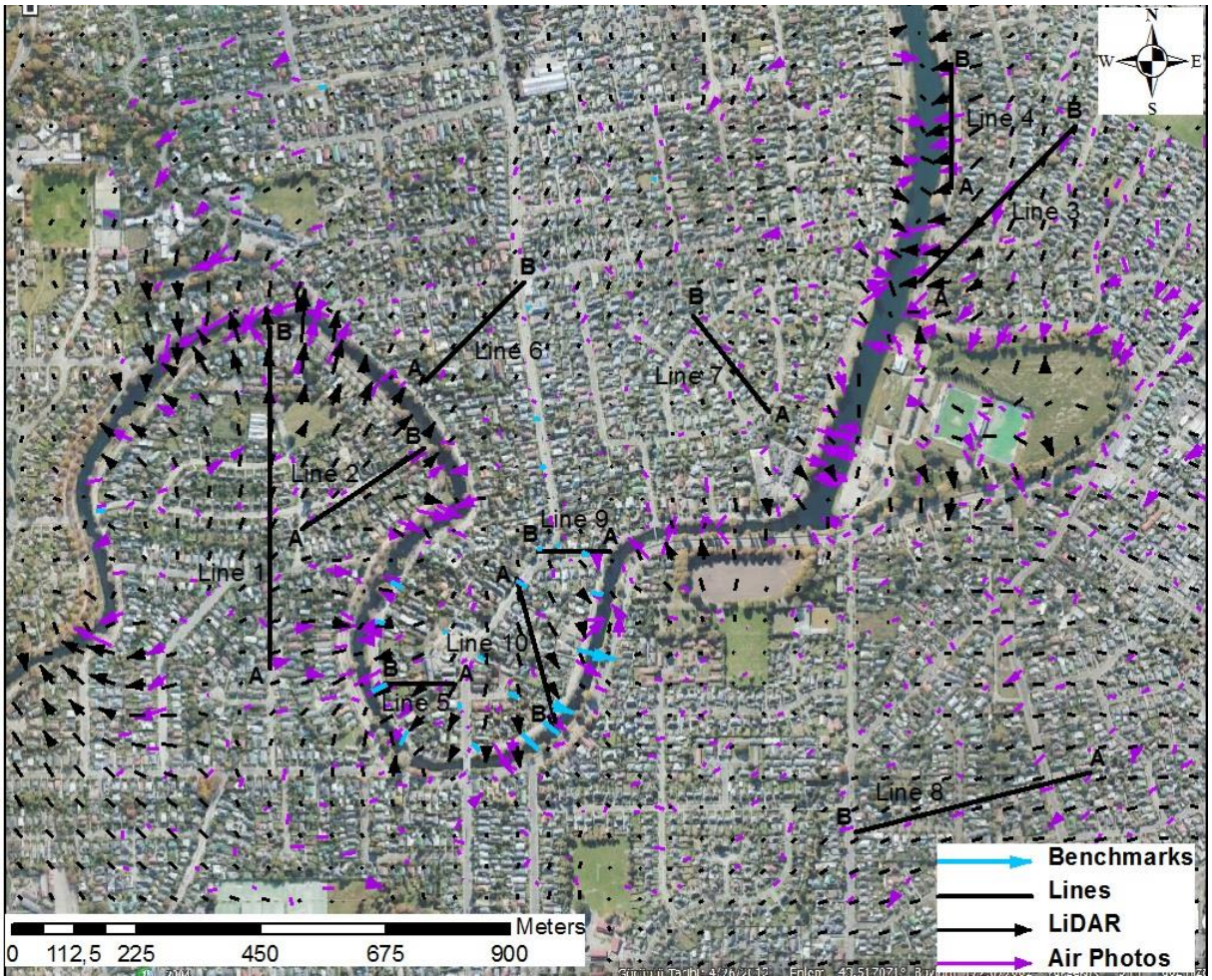

Figure 3. Lines along which LiDAR, Air photo and benchmark measurements are compared.

Figure 6 shows the comparison of LiDAR and air photo displacements with available benchmark measurements in Avonside area. Comparisons were made by using the displacement components in east-west and north-south directions. There are 25 benchmarks at this location. In the comparisons, the

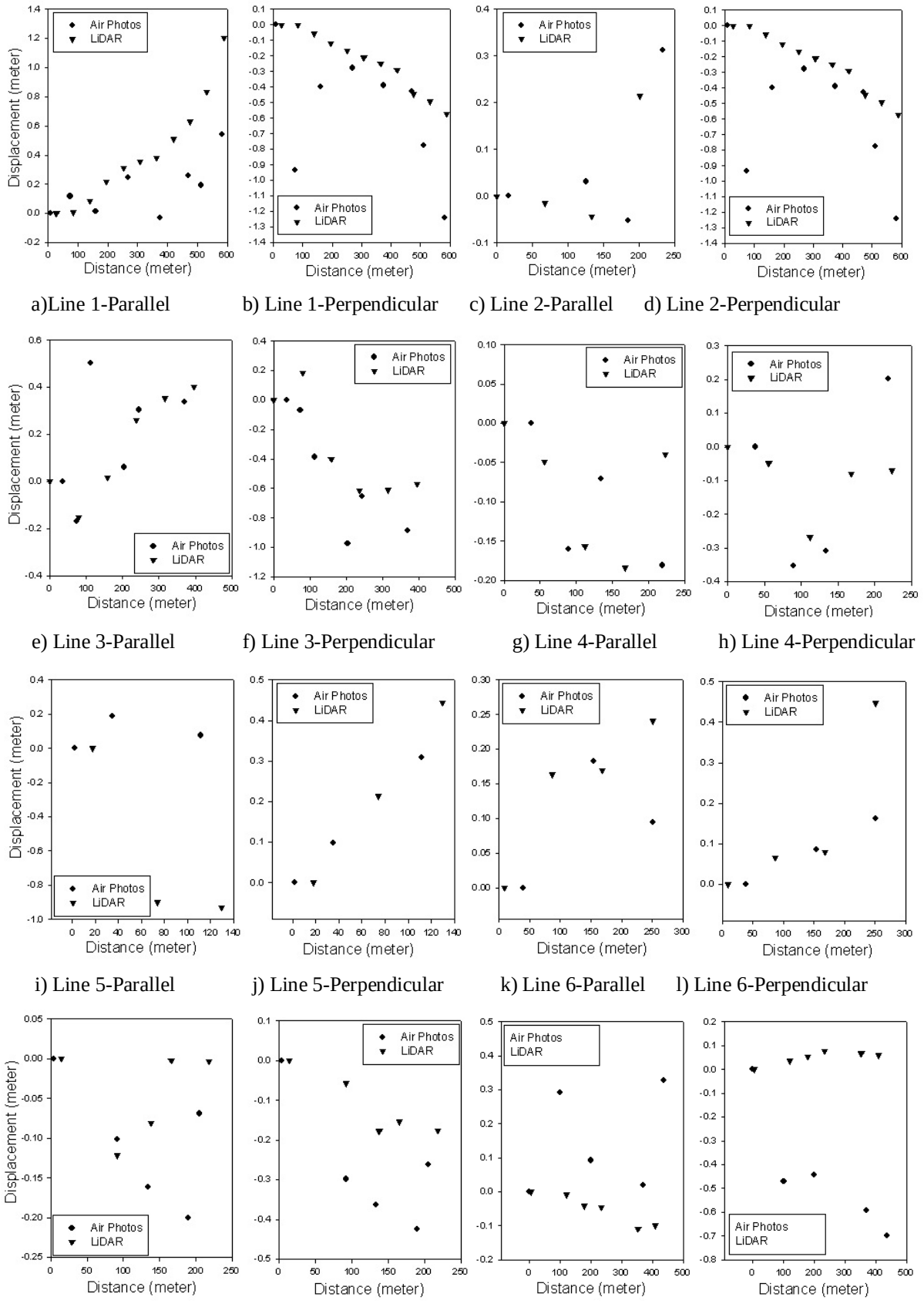

a)Line 1-Parallel b) Line 1-Perpendicular c) Line 2-Parallel d) Line 2-Perpendicular

e) Line 3-Parallel f) Line 3-Perpendicular g) Line 4-Parallel h) Line 4-Perpendicular

i) Line 5-Parallel j) Line 5-Perpendicular k) Line 6-Parallel l) Line 6-Perpendicular

m) Line 7-Parallel n) Line 7-Perpendicular o) Line 8-Parallel p) Line 8-Perpendicular

Figure 4. Comparison of parallel and perpendicular components of LiDAR and airphoto displacements for lines 1, 2, 3, 4, 5, 6, 7, and 8

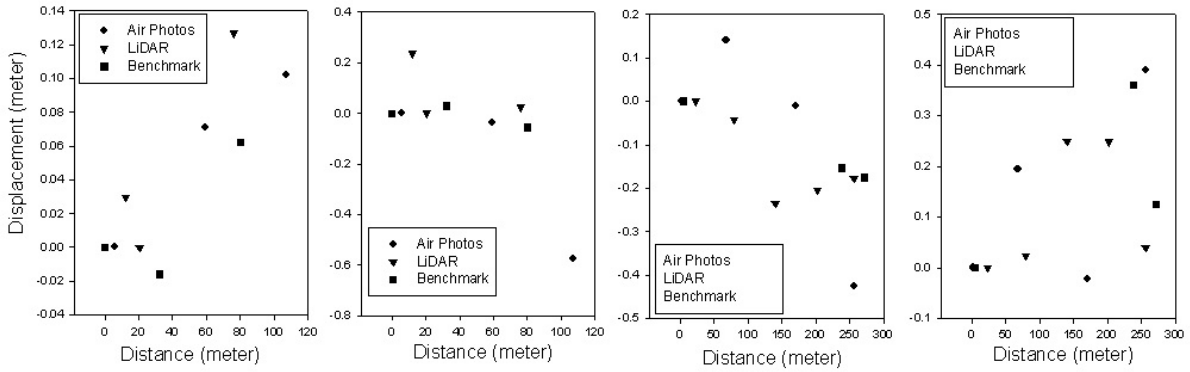

r) Line 9-Parallel s) Line 9-Perpendicular t) Line 10-Parallel u) Line 10-Perpendicular

Figure 5. Comparison of parallel and perpendicular components of LiDAR, airphoto, and benchmark displacements for lines 9 and 10

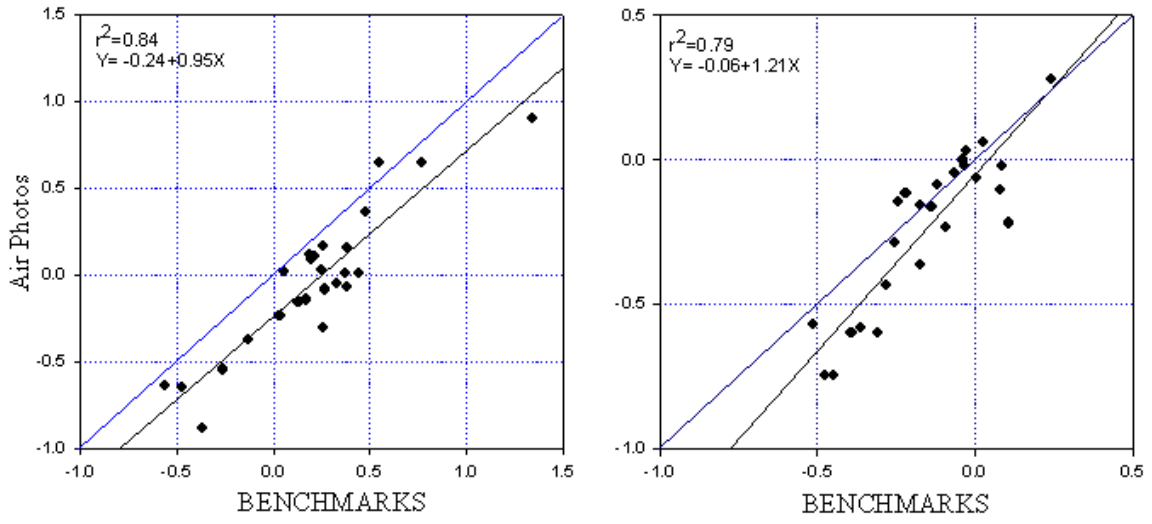

a) Benchmarks-Air Photos in east-west direction b) Benchmarks-Air Photos in north-south direction

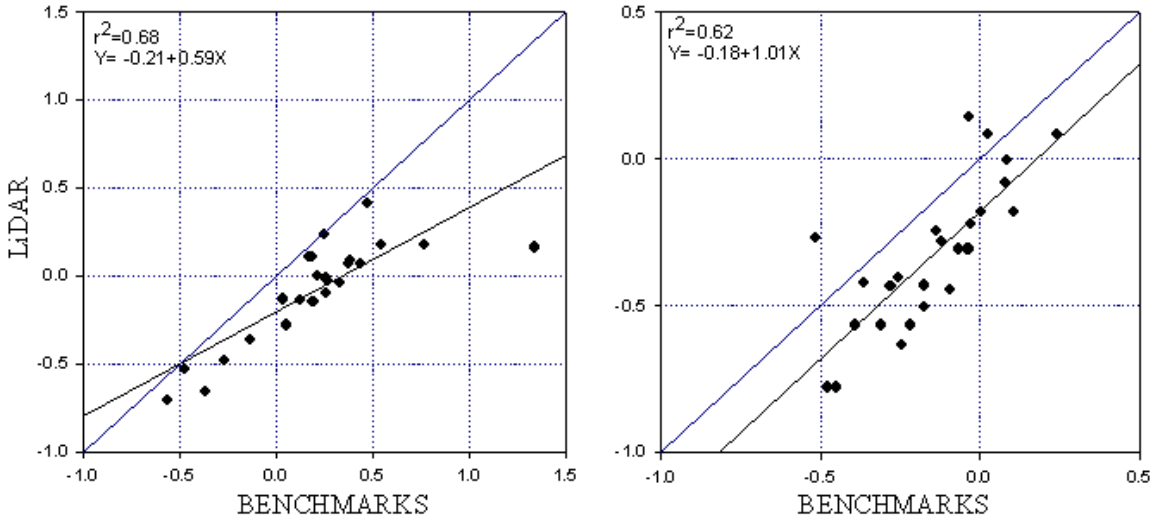

c) Benchmarks-LiDAR in east-west direction d) Benchmarks-LiDAR north-south direction

Figure 6. Comparison of benchmark displacement with LiDAR and airphoto displacements

closest LiDAR and airphoto measurement locations to the respective benchmark were selected. Figure 6 also shows the regression lines and r^2 values. When regressed against benchmark displacements air photo displacements provided higher r^2 (0.84 for east-west direction and 0.79 for north-south direction) than LiDAR displacements (0.68 for east-west direction and 0.62 for north-south direction).

Figure 7 shows the comparison of LiDAR and air photo displacements in east-west direction and north-south direction in Avonside area. The air photo displacements are direct calculated values from air surveys. The LiDAR displacement values were obtained at air photo measurement locations by using kriging interpolations of 56-m interval data. Only 652 air photo measurement locations out of 680 were used according to the procedure described in a later section. 28 air photo measurement locations were considered as anomalies. Comparisons show that there is a scatter in the data even though there are obvious trends.

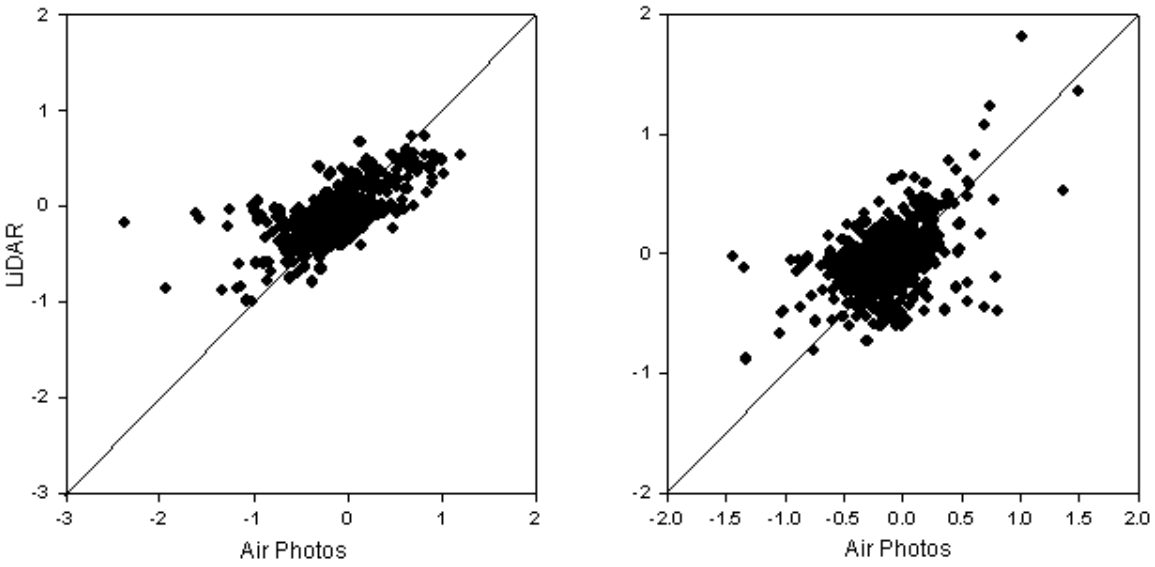

a) Air Photos- LiDAR in east-west direction b) Air Photos- LiDAR in north-south direction

Figure 7. Comparison of LiDAR and airphoto displacements

Pipeline Damage Relationships

Figure 1 shows the water pipelines and repair locations in Avonside area. Table 1 presents pipe length with respect to pipe materials as well as the pipe damages occurred after 22 February 2011 earthquake. In this study, the focus was on AC pipelines as the length of the pipelines and number of damages were much higher. The average repair rate for the AC pipelines in the study area is 6.61, which is about three times higher than the average repair rate (2.38) in liquefaction areas of Christchurch.

Table 1. Pipeline and damage information in Avonside area

Earthquakes	Pipe Material	Pipe Length (km)	Repairs	Overall Average RR
22 February 2011	AC	15,1	100	6,61
	CI	10,1	41	4,05
	PVC	3,4	29	8,49
	MPVC	0,6	0	0,00
	Other	4,3	25	5,87
	Total	33,5	200	5,97

For the purpose of horizontal strain calculations from LiDAR displacements, the horizontal displacement data points are considered as corners of square elements shown in Fig. 8. The grid with square elements may be regarded as a finite element mesh with bilinear quadrilateral elements. Knowing the coordinates of each corner and the corresponding displacement, the strains in the EW and NS directions (ε_x and ε_y, respectively) and shear strains (γ_{xy}) can be calculated by computing the spatial derivatives of displacements using linear interpolation. Accordingly, finite element formulations were used to determine horizontal ground strains in the center of the elements, following the method described by Cook (1995). The strain matrix is calculated from the 56 x 56m cell displacements as

$$\begin{Bmatrix} \varepsilon_x \\ \varepsilon_y \\ \gamma_{xy} \end{Bmatrix} = \frac{1}{4a^2} \begin{bmatrix} -(a-y) & 0 & (a-y) & 0 & \cdots \\ 0 & -(a-x) & 0 & -(a+x) & \cdots \\ -(a-x) & -(a-y) & -(a+x) & (a-y) & \cdots \end{bmatrix} \begin{Bmatrix} u_1 \\ v_1 \\ u_2 \\ v_2 \\ \vdots \\ v_4 \end{Bmatrix} \tag{1}$$

in which u_1, v_1, u_2,...,v_4 are the corner displacements defined in Fig. 8, x and y are coordinates in two dimensional space, and a is the length of the square cell that is 56 m. Using the strains from Eqn. 1, the principal strains, ε_1 and ε_2, were calculated from well-known strain transformations as

$$\varepsilon_{1,2} = \frac{\varepsilon_x + \varepsilon_y}{2} \pm \sqrt{\left(\frac{\varepsilon_x - \varepsilon_y}{2}\right)^2 + \left(\frac{\gamma_{xy}}{2}\right)^2} \tag{2}$$

For the purpose of horizontal strain calculations from air photo displacements, the similar procedure described above for the LiDAR displacements were used. However, since the air photo displacement data point locations are not evenly distributed like LiDAR ones, first an interpolation scheme was utilized. Ordinary kriging was used to obtain air photo displacements at the corners of 56 x 56m cells. During the process, it was found out that there were some inconsistent data points which distort the interpolations. In order to eliminate those points the following procedure was used. First, for each of 680 air photo data, an average value of the displacements in east-west and north-south direction within the 50 m of the point of interest was calculated. Then, the averages and the values of the displacements at that particular point were compared. If both east-west and north-south displacements were in opposite directions, then the particular data point was discarded. The same procedure was followed by using 60 m and 70 m zones. At the end, 28 points were considered as anomalies and eliminated resulting in 652 air photo data available for kriging process.

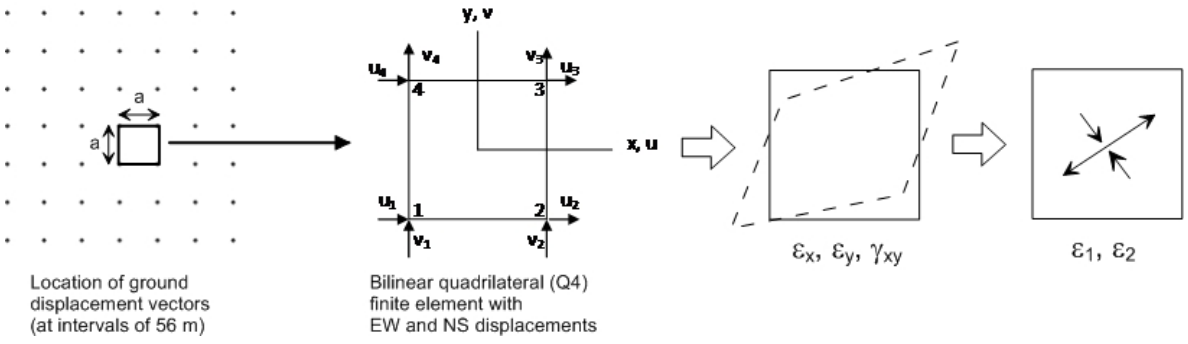

Figure 8. Procedure of calculating ground strains from horizontal ground displacements

Correlations of RR for different pipe types vs. lateral ground strains were developed by counting the number of repairs and pipeline lengths for the particular pipe type in each 56-m cell, and then calculating the RR associated with certain strain intervals. Figure 9 presents RR vs. lateral ground strain linear data and regressions for AC water pipelines for LiDAR and air photo measurements. The lateral ground strain is the maximum absolute value of the ground strain, $\mathring{U}_{HP}$, given by Eqn. 2. The RRs were screened following procedures described by OôRourke et al. (2014). As discussed in OôRourke et al. (2014), the fidelity of the RR statistics is sensitive to the pipeline length sampled and number of repairs observed within a given sampling length. To select lengths sufficient to produce meaningful correlations, models adopted by OôRourke et al. (2014) used herein.

$$x \geq [\phi^{-1}(\beta_c)]^2/\alpha^2(RR) \tag{3}$$

in which x is the sampling length; $\grave{\varepsilon}^{-1}(6_c)$ is confidence interval of 6_c and corresponding standard normal deviate ; Ŭis percentage of the true value; and RR is repair rate. Thus, the sampling criteria in Eqn. 3 are independent of sampling interval, and can be applied for any RR, including relatively small RRs related to TGD effects and large RRs related to PGD effects. For example, to select the minimum sampling length for a 90% confidence limit, Ŭ= 0.5, and RR = 1 repair/km, one determines ū -1(90%) = 1.645 and then uses Eqn. (3) to obtain 10.82 km. When screening the data, one will obtain a particular length of pipeline corresponding to a specific range of GMPGV, differential settlements, or lateral ground strain. If the repairs within that length result in RR = 1 repair/km, the sampling criteria requires that the length be equal to or greater than 10.82 km. Pipeline RR data were screened using Eqn. (3) with 90% confidence and Ŭ= 50% for LiDAR. To provide a sufficient number of data points for robust interpolation, the screening criteria associated with Eqn. 3 were relaxed to reflect a confidence of approximately 85% for the pipeline damage relationships from air photo displacements.

The r-squared values for the correlation between pipeline damage and lateral ground strains from LiDAR are higher than the correlation from air photo, indicating stronger correlation. The difference between the regressions is not so significant for lower strains and almost identical for higher strain values. The RRs plotted in Figure 9 also reflect damage from differential settlement that can occur even when $\mathring{U}_{HP}$ = 0, as shown in the regressions.

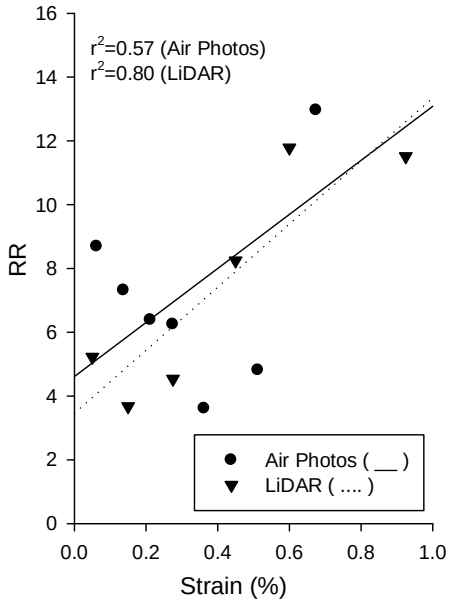

Figure 9. RR values obtained for AC pipelines from LiDAR and air photo measurements

CONCLUSIONS

This paper compares displacements measured in Avonside area, Christchurch, NZ, by using two different ways namely air photo and high resolution LiDAR surveys data acquired before and after the 6.2 MW 22 February 2011 earthquake with respect to their effects on pipeline damage assessments. At first, LiDAR, air photo and benchmark horizontal ground displacements were compared along the selected lines in Avonside area. The results show that there are reasonably good comparison between the displacements measured by LiDAR and air photo for many of the lines. But the differences are quite significant along few lines. Also there is more scatter in air photo displacements. When compared with benchmarks, no clear superiority is observed for LiDAR and air photo measurements. Regarding the correlation between pipeline damage and lateral ground strains, the difference between the regressions is not so significant for lower strains and almost identical for higher strain values.

ACKNOWLEDGEMENT

Partial grant provided by PAU BAP to attend the conference is acknowledged.

REFERENCES

Canterbury Earthquake Recovery Authority (CERA) (2012) ñGeotechnical database for Canterbury earthquake sequenceò https://canterburygeotechnicaldatabase.projectorbit.com

Cook RD (1995) Finite Element Modeling for Stress Analysis, John Wiley and Sons

Hamada M and OõRourke TD (1992) ñEds., Case Studies of Liquefaction and Lifeline Performance During Past Earthquakes,ò *Technical Report NCEER-92-0001, National Center for Earthquake Engineering Research*, State University of New York at Buffalo, NY, February

Hamada M, Yasuda S, Isoyama R, Emoto K (1986) ñStudy on Liquefaction Induced Permanent Ground Displacement.ò Association for the Development of Earthquake Prediction, Tokyo, Japan, November

Land Information New Zealand (LINZ, 2014) ñhttp://apps.linz.govt.nz/gdb/index.aspx?nextform=image&image_id=108377&mode=&sessionid= 1155552391588813977337 94&code=BDVBò

OõRourke TD, Jeon SS, Toprak S, Cubrinovski M, Hughes M, Ballegooy S, Bouziou D (2013) ñEarthquake Response of Underground Pipeline Networks in Christchurch, NZò, *Earthquake Engineering Research Institute, EERI*

O'Rourke TD, Jeon SS, Toprak S, Cubrinovski M, Jung JK (2012) ñUnderground Lifeline System Performance during the Canterbury Earthquake Sequenceò, *15th World Conference in Earthquake Engineering*, Lisbon, Portugal, September

Toprak S, Nacaroglu E, Koç AC (2011) ñSeismic Damage Probabilities for Segmented Buried Pipelinesò, *Applications of Statistics and Probability in Civil Engineering* ï Faber, Köhler & Nishijima (eds), ETH Zurich, Switzerland, 2-4 August, 2199-2203

Toprak S, Taskin F, Koc AC (2009) ñPrediction Of Earthquake Damage To Urban Water Distribution Systems: A Case Study For Denizli, Turkeyò, *The Bulletin of Engineering Geology and the Environment*, 68:499-510